Structure and predissociation of the 3p sigma D-u (3)Sigma(+)(u) Rydberg state of N2: First extreme-ultraviolet and new near-infrared observations, with coupled-channels analysis

Lewis, B.R.; Baldwin, K.G.H.; Heays, A.N.; Gibson, S.T.; Sprengers, J.P.; Ubachs, W.M.G.; Fujitake, M.

published in
Journal of Chemical Physics
2008

DOI (link to publisher)
10.1063/1.3023034

document version
Publisher's PDF, also known as Version of record

Structure and predissociation of the $3p\sigma_u D\ ^3\Sigma_u^+$ Rydberg state of N_2: First extreme-ultraviolet and new near-infrared observations, with coupled-channels analysis

B. R. Lewis,[1,a)] K. G. H. Baldwin,[1] A. N. Heays,[1] S. T. Gibson,[1] J. P. Sprengers,[2] W. Ubachs,[2] and M. Fujitake[3]

[1]*Research School of Physical Sciences and Engineering, The Australian National University, Canberra, Australian Capital Territory 0200, Australia*

[2]*Department of Physics and Astronomy, Laser Centre, Vrije Universiteit, De Boelelaan 1081, 1081 HV Amsterdam, The Netherlands*

[3]*Department of Physics, Kanazawa University, Kakuma, Kanazawa 920-11, Japan*

(Received 21 September 2008; accepted 22 October 2008; published online 24 November 2008)

The $3p\sigma_u D\ ^3\Sigma_u^+$ Rydberg state of N_2 is studied experimentally using two high-resolution spectroscopic techniques. First, the forbidden $D\ ^3\Sigma_u^+ - X\ ^1\Sigma_g^+$ transition is observed for the first time via the (0,0) band of $^{14}N_2$ and the (1,0) band of $^{15}N_2$, using 1 extreme-ultraviolet +1 ultraviolet two-photon-ionization laser spectroscopy. Second, the Rydberg–Rydberg transition $D\ ^3\Sigma_u^+ - E\ ^3\Sigma_g^+$ is studied using near-infrared diode-laser photoabsorption spectroscopy, thus extending the previous measurements of Kanamori *et al.* [J. Chem. Phys. **95**, 80 (1991)], to higher transition energies, and thereby revealing the (2,2) and (3,3) bands. The combined results show that the $D(v=0-3)$ levels exhibit rapidly increasing rotational predissociation as v increases, spanning nearly four orders of magnitude. The D-state level structure and rotational predissociation signature are explained by means of a coupled-channels model which considers the electrostatically coupled $^3\Pi_u$ Rydberg-valence manifold, together with a pure-precession **L**-uncoupling rotational interaction between the $3p\sigma_u D\ ^3\Sigma_u^+$ and $3p\pi_u G\ ^3\Pi_u$ Rydberg p-complex components. © *2008 American Institute of Physics*. [DOI: 10.1063/1.3023034]

I. INTRODUCTION

There has recently been a resurgence of activity in the experimental and theoretical study of the extreme-ultraviolet (XUV) spectroscopy and predissociation dynamics of molecular nitrogen. This has been driven not only by the desire to gain a fundamental understanding of this complex spectral region of strongly interacting, closely spaced Rydberg and valence electronic states, but also by the importance of this understanding to the solution of topical problems in planetary-atmospheric physics and chemistry. For example, a new coupled-channel Schrödinger-equation (CSE) model of N_2 isotopic photodissociation has recently been successful in explaining the N-isotope anomaly in HCN in Titan's atmosphere.[1] Predissociation of the dipole-accessible singlet states of N_2 is controlled ultimately by the triplet manifold,[2] so a detailed knowledge of the triplet-state predissociation mechanism is essential for a realistic understanding of the molecular dissociation process.

The $3p\sigma_u D\ ^3\Sigma_u^+$ state of N_2, well known for many years as the upper state of the fourth positive emission system, $D\ ^3\Sigma_u^+ \rightarrow B\ ^3\Pi_g(0,v'')$,[3] is the first member of a Rydberg series converging on the $X\ ^2\Sigma_g^+$ state of N_2^+. The $D(v=0)$ level has also been observed, albeit at very low resolution, in both electron threshold excitation[4] and dissociative-charge-transfer kinetic-energy release[5] spectra. In a ground-breaking 1991 study, Kanamori *et al.*[6] observed both the (0,0) and (1,1) bands of the dipole-allowed $3p\sigma_u D\ ^3\Sigma_u^+ \leftarrow 3s\sigma_g E\ ^3\Sigma_g^+$ Rydberg–Rydberg system in $^{14}N_2$, using high-resolution near-infrared (NIR) diode-laser photoabsorption spectroscopy, allowing the fine structure of both states to be characterized for the first time. In addition, while the $D(v=0)$ level was found to be unpredissociated, significant rotational predissociation was observed in the $D(v=1)$ level.[6]

Theoretical studies on the D state are relatively few. Lefebvre-Brion and Moser[7] and Cremaschi *et al.*[8] have calculated excitation energies for many Rydberg states of N_2, including the D state, while *ab initio* potential-energy curves have been computed by Michels[9] and Minaev *et al.*[10] Although these latter studies indicate that the D state undergoes an avoided crossing with the repulsive $3\ ^3\Sigma_u^+$ valence state on its outer limb, both imply that there should be several levels above $v=1$ accessible in the D state before significant electrostatic predissociation sets in due to this interaction. The spin-forbidden $D\ ^3\Sigma_u^+ - X\ ^1\Sigma_g^+$ transition, occurring in the XUV, has not been seen previously. However, Minaev *et al.*[10] calculated an oscillator strength of 2.0×10^{-5} for the $D-X(0,0)$ band, suggesting that it may be observable experimentally.

In the present work, we report the first optical observations of the $D\ ^3\Sigma_u^+ - X\ ^1\Sigma_g^+$ transition, using high-resolution 1 XUV+1 UV two-photon-ionization laser spectroscopy, recording spectra for the (0,0) band in $^{14}N_2$ and the (1,0) band in $^{15}N_2$. These bands become observable due to intensity borrowing from the dipole-allowed $^1\Pi_u - X\ ^1\Sigma_g^+$ transi-

a)Electronic mail: brenton.lewis@anu.edu.au.

tions via local $D\ ^3\Sigma_{u1}^+ \sim\ ^1\Pi_{u1}$ spin-orbit interactions, a mechanism similar to that allowing the recent observation of several $^3\Pi_u - X\ ^1\Sigma_g^+$ transitions in the same molecule.[11,12] In addition, we report the first observations of the $D(v=2,3)$ levels, using high-resolution NIR diode-laser photoabsorption spectroscopy to record the $D\ ^3\Sigma_u^+ \leftarrow E\ ^3\Sigma_g^+(2,2)$ and (3,3) bands of $^{14}N_2$. Finally, the pattern of rapidly increasing rotational predissociation found in the $D(v=0-3)$ levels is explained using a CSE model of the interacting $^3\Sigma_u^+$ and $^3\Pi_u$ states of N_2.

II. EXPERIMENTS

A. XUV spectroscopy

The present laser-based XUV source has been used in previous experimental studies of N_2 transition energies and linewidths and has been described in detail elsewhere.[13,14] Briefly, the sixth harmonic of either a pulsed dye laser (PDL) or pulsed dye amplifier (PDA) was employed. Both the PDL and PDA were pumped by the second harmonic of a pulsed Nd:YAG (yttrium aluminum garnet) laser, with the PDA also seeded by the output of a tunable cw ring dye laser, in turn pumped by the output of a 532 nm Millennia-V laser. In both systems, UV radiation was generated by frequency doubling the visible radiation in a KD^*P crystal, while subsequent frequency tripling of the UV in a xenon gas jet produced the XUV radiation. The XUV beam was crossed with a pulsed and skimmed N_2 jet and the ions formed in the 1 XUV +1 UV two-photon-ionization process were accelerated in a time-of-flight setup to the electron-multiplier detector.

Absolute frequency calibration was performed in the visible using I_2 absorption (PDL) or saturated-absorption (PDA) spectroscopy.[13,14] The absolute wavenumber uncertainty for the lines recorded with the PDL-based XUV system is $\pm 0.2\ \text{cm}^{-1}$, while for the PDA-based source the uncertainty is $\pm 0.003\ \text{cm}^{-1}$. For those PDA spectra showing significant Doppler broadening, the uncertainty increases to $\pm 0.02\ \text{cm}^{-1}$. The ultimate instrumental resolution obtainable with the PDA-based source and the lowest-temperature jet configuration was $\sim 0.01\ \text{cm}^{-1}$ full width at half maximum (FWHM), including the Doppler component.

Some of the PDA-based measurements were performed with a gas-jet nozzle-skimmer distance of 150 mm to reduce the Doppler broadening. However, in this configuration, due to the low rotational temperature in the gas expansion, only low-rotational levels were populated and only levels with $J \leq 5$ were studied. To observe higher-J levels, the nozzle-skimmer distance was reduced to 0 mm to increase the signal sensitivity and the rotational temperature of the gas jet, producing, however, also a significant increase in Doppler broadening.[14]

B. NIR spectroscopy

The present apparatus, used previously in NIR photoabsorption studies of the $3p\pi_u c\ ^1\Pi_u \leftarrow 3s\sigma_g a''\ ^1\Sigma_g^+(1,0)$ Rydberg–Rydberg band of $^{14}N_2$, has been described in detail elsewhere.[15] Briefly, an external-cavity diode laser with piezoelectric cavity tuning was used as the radiation source for the NIR spectrometer. Wavenumber calibration was provided by a combination of a wavemeter, itself calibrated against H_2O absorption lines measured with a Fourier-transform spectrometer installed at Nobeyama Radio Observatory, and an étalon with a free spectral range of $\sim 0.025\ \text{cm}^{-1}$. The laser beam was divided into three beams by using two beam splitters. The principal beam passed through a multipass hollow-cathode discharge cell, with effective length 28 m, which was used for the photoabsorption studies on metastable N_2, while the others entered the wavemeter and étalon, respectively. The N_2 Rydberg states were generated by modulating the discharge at 8 kHz in a flowing mixture of 40 mTorr of N_2 and 600 mTorr of He, with the cell pumped continuously by a mechanical booster pump, followed by a rotary pump. The radiation transmitted through the discharge cell was detected at the modulation frequency using the phase-sensitive detection technique.

The spectral resolution achieved was limited by Doppler broadening to $\sim 0.024\ \text{cm}^{-1}$ FWHM, while the uncertainty in the determination of transition wavenumbers was $\sim 0.002\ \text{cm}^{-1}$ for the narrowest unblended lines, but larger for diffuse or blended lines. Line positions and Lorentzian (predissociation) linewidths were determined by least-squares fitting a synthetic spectrum comprising summed Voigt profiles to specific regions of the experimental absorption spectrum with the Gaussian component of the profile fixed at the Doppler contribution.

III. THEORETICAL METHOD

The strongest interaction involving the $D\ ^3\Sigma_u^+$ state, which is likely to lead to predissociation, is electrostatic coupling to the repulsive $3\ ^3\Sigma_u^+$ valence state. However, as mentioned in Sec. I, the avoided crossing between these two states occurs high on the outer limb of the D-state potential-energy curve[9,10] in a position unlikely to affect the D-state levels that are the subject of this work. In any case, this homogeneous interaction would be incapable of causing the strong heterogeneous predissociation seen in $D(v=1)$ by Kanamori *et al.*[6] and the further examples in $D(v=2,3)$ reported here. The $3p\sigma_u D\ ^3\Sigma_u^+$ state is a member of the $3p$ Rydberg complex, itself the lowest member of a series converging on the $X\ ^2\Sigma_g^+$ (ground) state of N_2^+. The other complex members are $3p\sigma_u c'\ ^1\Sigma_u^+$, $3p\pi_u c\ ^1\Pi_u$, and $3p\pi_u G\ ^3\Pi_u$. Direct predissociation of the Rydberg D state by a valence state of different symmetry is unlikely to be a significant process. However, the $3p\sigma_u D\ ^3\Sigma_u^+$ state undergoes a first-order $\mathbf{L}$-uncoupling interaction with the $3p\pi_u G\ ^3\Pi_u$ complex member, which is likely to be the driving mechanism behind an indirect heterogeneous predissociation of the D state since the heavily coupled $^3\Pi_u$ manifold is itself strongly predissociated by the $C'\ ^3\Pi_u$ valence state.[2]

Because of the multilevel nature of this indirect predissociation mechanism, it is necessary to employ the CSE technique[16] to model the interactions between the $D\ ^3\Sigma_u^+$ state and the $^3\Pi_u$ manifold. Briefly, the diabatic-basis coupled-channel radial Schrödinger equation for the coupled states is solved numerically to yield the coupled-channel wave function for the excited state, which is then used together with the ground-state radial wave function and a

nominal diabatic $D-X$ electronic transition moment to form the total photodissociation cross section.[17] D-state transition energies and predissociation linewidths derived from the computed cross section by Fano-profile fitting are then compared iteratively with the experimental values in order to optimize the CSE-model parameters. Rotational calculations are performed by including an appropriate centrifugal term in the Hamiltonian, while isotopic calculations require changing only the value of the reduced molecular mass μ in the CSE model.

The specific model basis employed here includes the $3p\sigma_u D\ ^3\Sigma_u^+$, $3p\pi_u G\ ^3\Pi_u$, and $3s\sigma_g F\ ^3\Pi_u$ Rydberg states together with the $C\ ^3\Pi_u$ and $C'\ ^3\Pi_u$ valence states. The $^3\Pi_u$ part of the model has been discussed in detail in Ref. 18 and is unchanged here, except for the necessary inclusion of all Ω components, with appropriate spin-orbit splitting[12,19] and **S**-uncoupling[20] within the manifold. Separate calculations are performed for each J value, and for both the e- and f-parity blocks in a Hund's case-(a) basis.[21]

The main model parameters of interest here are the potential-energy curve for the $D\ ^3\Sigma_u^+$ state and its couplings to the $G\ ^3\Pi_u$ state. Expressions for the $^3\Sigma_\Omega \sim {}^3\Pi_{\Omega'}$ substate interactions have been well documented[20,22–24] and are controlled by two relevant electronic couplings, $\xi = \langle {}^3\Pi_1 | \mathbf{H}^{SO} | {}^3\Sigma_1 \rangle$, and $\eta = \langle {}^3\Pi_2 | \mathbf{L}^+ | {}^3\Sigma_1 \rangle$, where $\mathbf{H}^{SO}$ and $\mathbf{L}^+$ are the spin-orbit operator and the J-independent part of the **L**-uncoupling operator, respectively. In the present CSE model, the dependences of these operators on the internuclear distance R are neglected, and the constants ξ and η together with the D-state potential-energy curve are the only parameters varied in the comparison between the model and experiment. In this approximation, the full **L**-uncoupling interactions take the form $-\eta B(R)\sqrt{[J(J+1)-\Omega(\Omega+1)]}$,[25] where $B(R)=\hbar^2/(2\mu R^2)$.[21]

IV. RESULTS AND DISCUSSION

A. XUV experiment

1. $D(v=0)$ in $^{14}N_2$

Using the PDL-based and PDA-based XUV sources, the spin-forbidden $D\ ^3\Sigma_u^+ - X\ ^1\Sigma_g^+(0,0)$ transition was observed in $^{14}N_2$. A PDL-based spectrum of the $D-X(0,0)$ band is shown in Fig. 1, its fortuitous location, in a relatively clear region of the allowed spectrum just above the $b-X(4,0)$ band head, enabling its clear observation. The three sublevels for Hund's case-(b) $^3\Sigma_u^+$ states, F_1 ($J=N+1$, f parity), F_2 ($J=N$, e parity), and F_3 ($J=N-1$, f parity), give rise to four rotational branches, R, P, ^RQ, and ^PQ, in electronic transitions from $^1\Sigma_g^+$ (e parity) states in accordance with rotational and parity selection rules. All of these branches occur in the $D-X(0,0)$ band, as verified in Fig. 2, which shows PDA-based spectra in the region of the $R(4)+{}^RQ(4)$ and $P(2)+{}^PQ(2)$ lines. The experimental resolution of these line pairs allows the determination of the $D(v=0)$ fine-structure splitting. The $D-X(0,0)$ rotational-branch transition energies determined from all spectra, together with the corresponding $D(v=0)$ rotational term values calculated using X-state terms derived from the spectroscopic parameters of Bendtsen,[26] are summarized in Table I.

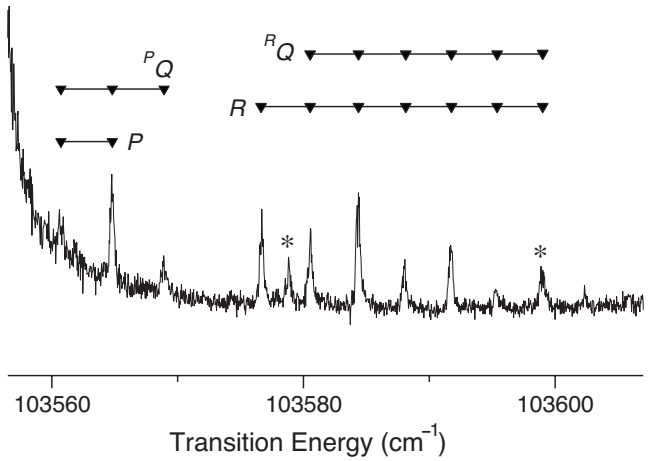

FIG. 1. 1 XUV+1 UV ionization spectrum of the $D\ ^3\Sigma_u^+ - X\ ^1\Sigma_g^+(0,0)$ band in $^{14}N_2$, recorded using the PDL-based XUV source. The rising signal level at the extreme left of the spectrum is from the band head of the much stronger $b\ ^1\Pi_u - X\ ^1\Sigma_g^+(4,0)$ transition. The lines marked with an asterisk are high-rotational lines from the $c\ ^1\Pi_u - X\ ^1\Sigma_g^+(0,0)$ band.

Spectroscopic parameters for the $D(v=0)$ level in $^{14}N_2$, determined by fitting the PDA-derived rotational term values in Table I to the $^3\Sigma$ Hamiltonian of Cheung *et al.*,[27] are listed in the second column of Table II. The present rotational and splitting parameters are in excellent agreement with the more precise values of Kanamori *et al.*[6] except that the present D_v value is not determined well since only low-N levels have been studied. However, this is the first time that the $D-X$ transition has been observed optically and the present data give the first absolute band origin for $D-X(0,0)$ in $^{14}N_2$.

No predissociation broadening of the $D(v=0,J)$ levels was observed in the present study, with all linewidths instrument limited. Kanamori *et al.*[6] also failed to observe predissociation broadening in their study, which was performed with a superior resolution, limiting any broadening to $\lesssim 0.002$ cm^{-1} FWHM. Kurzweg *et al.*[28] measured a (rotationally averaged) lifetime of 14.1 ± 1.0 ns for the $D(v=0)$

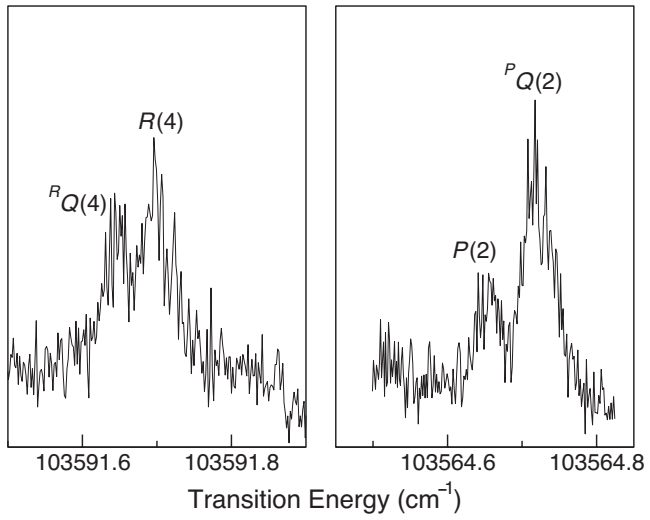

FIG. 2. 1 XUV+1 UV ionization spectrum of the $D\ ^3\Sigma_u^+ - X\ ^1\Sigma_g^+(0,0)$ band in $^{14}N_2$, recorded using the PDA-based XUV source, emphasizing the fine-structure splitting of the $D(v=0)$ level. Left: Recording of $^RQ(4)$ and $R(4)$. Right: Recording of $P(2)$ and $^PQ(2)$.

TABLE I. Observed transition energies for the $D\ ^3\Sigma_u^+ - X\ ^1\Sigma_g^+(0,0)$ band in $^{14}N_2$ and corresponding $D(v=0)$ term values, all in cm^{-1}. Entries given to three decimal places are from PDA spectra, those to two decimal places from PDL spectra. Entries marked with an asterisk are derived from blended lines.

J''	$R(J'')$	$^RQ(J'')$	$^PQ(J'')$	$P(J'')$	N'	$T_1(N')$	$T_2(N')$	$T_3(N')$
0	103 576.587				0	103 572.713		
1	103 580.452*	103 580.452*	103 568.734		1	103 576.654	103 576.589	
2	103 584.259*	103 584.259*	103 564.717	103 564.654	2	103 584.59*	103 584.431*	103 584.431*
3	103 588.002	103 587.978	103 560.72*	103 560.72*	3		103 596.196*	103 596.196*
4	103 591.697	103 591.647			4		103 611.876	103 611.852
5	103 595.323	103 595.256			5		103 631.486	103 631.436
6	103 599.01*	103 599.01*			6		103 655.005	103 654.938
8	103 605.66*	103 605.66*			7		103 682.56*	103 682.56*
10	103 612.53*	103 612.53*			9		103 748.88*	103 748.88*
					11		103 831.31*	103 831.31*

level in $^{14}N_2$, corresponding to a total linewidth of $\sim 0.0004\ cm^{-1}$ FWHM, which is consistent with the lack of observation of predissociation in the two experiments.

2. $D(v=1)$ in $^{15}N_2$

In the case of $^{15}N_2$, the $D-X(0,0)$ band was not observed. However, the (1,0) band was observed in association with a level crossing between $D\ ^3\Sigma_u^+(v=1)$ and $o\ ^1\Pi_u(v=0)$. In this isotopomer, the Rydberg level $D(v=1)$ lies a little below the valence level $o(v=0)$ with a significantly greater B value, leading to the level crossing and an associated local perturbation in $o(v=0)$, indicating significant effective singlet-triplet interaction. Because of the intensity borrowing due to this interaction, lines from the $D\ ^3\Sigma_u^+ - X\ ^1\Sigma_g^+(1,0)$ band are visible between lines from the dipole-allowed $o\ ^1\Pi_u - X\ ^1\Sigma_g^+(0,0)$ band, in the perturbed regions of the spectrum. This is illustrated in Fig. 3, where a 1 XUV +1 UV ionization spectrum of the R-branch regions of the $o-X(0,0)$ and $D-X(1,0)$ bands is shown. Line positions and line assignments for the $o-X(0,0)$ band have been given in Ref. 13. Those for the $D-X(1,0)$ band are given in Table III.

As shown in Fig. 4, where experimental reduced term values for $o(v=0)$ and $D(v=1)$ near the crossing region are presented (symbols), only the F_2 ($\Omega=1$, e parity) levels of $D\ ^3\Sigma_u^+(v=1)$ cross the $o\ ^1\Pi_u(v=0)$ level, near $J=4$. Therefore, only the e-parity levels of $o(v=0)$ are perturbed strongly, leading to the R and P branches of the $o-X(0,0)$ band showing an irregular structure that is not present in the Q branch. For example, the $R(2)$ and $R(3)$ lines are very close to each other, and are just resolved in the lower XUV spectrum of Fig. 3. Furthermore, the F_2 levels of $D(v=1)$ are more strongly mixed with $o(v=0)$ than the F_1 and F_3 (f parity) levels. Therefore, the transitions accessing those levels (R and P branches, $e-e$ parity) borrow much more intensity than the transitions to the F_1 and F_3 levels. In fact, only two very weak lines accessing the F_1 and F_3 levels of $D(v=1)$ have been observed, $^PQ(1)$ and $^RQ(1)$.

In order to extract spectroscopic parameters for $D(v=1)$, a local deperturbation analysis has been performed by considering both parity components of each level, together with an effective interaction H_{12} between the $\Omega=1$ components of $D(v=1)$ and $o(v=0)$. As in Sec. IV A 1, the unperturbed $D(v=1)$ energies were described by the $^3\Sigma$ Hamiltonian of Cheung *et al.*,[27] while those for $o(v=0)$ were represented by the usual polynomials, including a two-parameter expression for the Λ-doubling. Thus, a 2×2 interaction matrix was required for the e-parity block and a 3×3 matrix for the f-parity block with a common singlet-triplet interaction parameter H_{12}. The resultant deperturbed

TABLE II. Fitted spectroscopic parameters for the $D(v=0-3)$ levels of N_2, all in cm^{-1}. 1σ fitting uncertainties are given in parentheses, in units of the last significant figure. The $^{14}N_2$, $D(v=0)$ and $^{15}N_2$, $D(v=1)$ parameters are derived from the present XUV spectra, the remainder from the present NIR spectra.

Parameter	$^{14}N_2$, $D(v=0)$	$^{15}N_2$, $D(v=1)$ [a]	$^{14}N_2$, $D(v=1)$ [b]	$^{14}N_2$, $D(v=2)$	$^{14}N_2$, $D(v=3)$
B	1.9609(6)	1.7603(4)	1.8828(2)	1.842(2)	1.843(3)
$D\times 10^5$	1.1(12)	1.0(7)	1.04(4)	1.0[c]	1.0[c]
λ	−0.036(6)	−0.065(4)	−0.053(10)	−0.031(11)	−0.022(12)
λ_D			−0.000 59(7)		
γ	0.018(2)	0.006(2)	0.0287(10)	0.020(3)	0.007(4)
γ_D			−0.000 042(5)		
$\nu_0[D-X(v,0)]$	103 572.709(7)	105 641.80(1)			
$\nu_0[D-E(v,v)]$			7752.260(7)	7698.56(1)	7634.86(1)
σ_{fit}	0.003[d]	0.002	0.03	0.03	0.02
N_{max}	6	7	19	7	4

[a]Two-level-deperturbed values. $H_{12}=0.910(5)+0.0054(3)J(J+1)\ cm^{-1}$.
[b]Parameters deduced from terms of Ref. 6 and the present NIR work.
[c]Parameter fixed in fit.
[d]Excludes blended lines. $\sigma_{fit}=0.005\ cm^{-1}$ rms, if included.

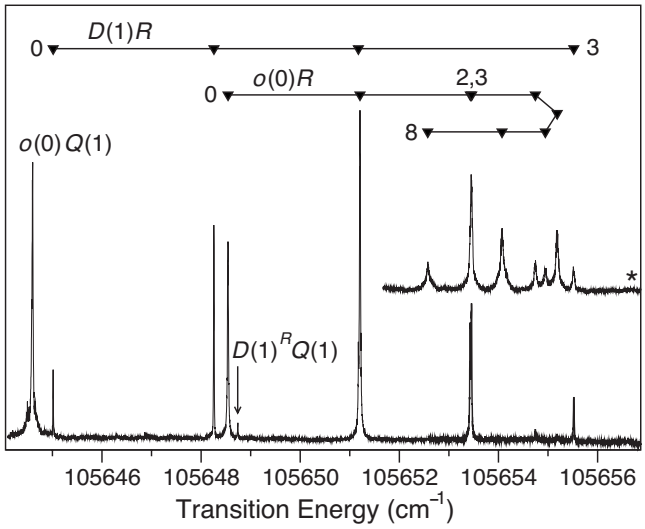

FIG. 3. 1 XUV+1 UV ionization spectrum of the R branches of the $o\ ^1\Pi_u - X\ ^1\Sigma_g^+(0,0)$ and $D\ ^3\Sigma_u^+ - X\ ^1\Sigma_g^+(1,0)$ bands in $^{15}N_2$, recorded using the PDA-based XUV source. Nozzle-skimmer distance=150 mm, except for the scan labeled with an asterisk where the nozzle-skimmer distance =0 mm.

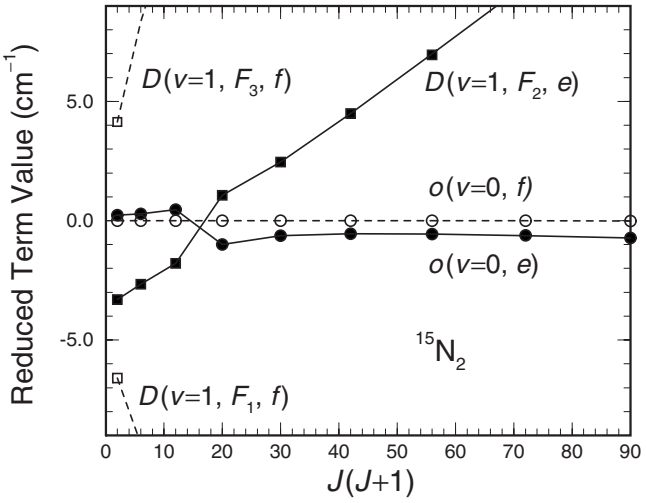

FIG. 4. Experimental reduced term values for e- and f-parity levels in the region of the $o(v=0) \sim D(v=1)$ crossing in $^{15}N_2$ (symbols). Terms have been reduced so that the $o(v=0)$ f-parity levels lie on the zero line. The two $D(v=1,f)$ level series, which are located above (F_3) and below (F_1) the $D(v=1,e)$ level series, do not cross $o(v=0)$ in the region covered by the figure. The fitted reduced terms resulting from the deperturbation procedure (see text) are also shown (solid lines: e levels and dashed lines: f levels).

spectroscopic parameters for $D(v=1)$ are given in the third column of Table II, with the value of H_{12} in footnote a, while the fitted perturbed reduced terms (curves) are compared with the experimental values in Fig. 4.

The present $^{15}N_2$ origin in Table II, taken together with the energy for $D(v=1)$ of $^{14}N_2$ quoted by van der Kamp *et al.*[5] and the ground-state isotope shift of 39.6 cm^{-1}, yield an experimentally based upper-state isotope shift of ~ 110 cm^{-1}, a value in agreement with expectation for the $v=1$ level of a member of a Rydberg series converging on the ground state of the molecular ion. Similarly, the ratio of the present B value in Table II and the value reported by Kanamori *et al.*[6] for the $D(v=1)$ level of the normal isotopomer, $B^{15}/B^{14}=0.9345$, is also in good agreement with the expected value, $\rho^2=\mu^{14}/\mu^{15}=0.9335$.[29] Thus, the $D(v=1)$ assignment for the level of $^{15}N_2$ observed here for the first time is confirmed unambiguously.

The splitting parameters, λ and γ, returned by the fitting procedure, differ somewhat from those found by Kanamori *et al.*[6] for the same vibrational level in $^{14}N_2$, but are of the same order of magnitude and sign. Since only one F_1 and one F_3 level are observed here, the reliability of the present splitting parameters may be questionable. In fact, it was only possible to determine values of λ and γ somewhat reliably in the fitting procedure by allowing a small rotational dependence in the coupling matrix element H_{12} (see Table II, footnote a). The observation of additional F_1 and F_3 levels would be highly desirable in order to resolve this issue unambiguously.

Kanamori *et al.*[6] found significant heterogeneous predissociation in the $D(v=1)$ level of $^{14}N_2$ with fitted Lorentzian linewidth components increasing quadratically with J. Predissociaton linewidth data for the $o(v=0)$ rotational levels in $^{15}N_2$ relevant to the present study have been presented elsewhere.[14] In summary, the low-J Lorentzian component of the $o(v=0)$ linewidth is around 0.016 cm^{-1} FWHM with evidence of a significant decrease at the culmination of the local perturbation near $J=4e$. In the case of the $D(v=1)$ perturber, we were unable to detect any broadening in excess of the instrumental contribution for the lowest levels studied in the low-temperature PDA-based spectra, i.e., $J=1$, $N=0,1,2$. However, a significant Lorentzian width of 0.009 ± 0.001 cm^{-1} FWHM was found for the $R(3)$ line. Us-

TABLE III. Observed transition energies for the $D\ ^3\Sigma_u^+ - X\ ^1\Sigma_g^+(1,0)$ band in $^{15}N_2$, together with corresponding $D\ ^3\Sigma_u^+(v=1)$ term values, all in cm^{-1}. Entries given to three decimal places are from PDA spectra, those to two decimal places from PDL spectra. Entries marked with an s are derived from shoulders in the spectrum.

J''	$R(J'')$	$^RQ(J'')$	$^PQ(J'')$	$P(J'')$	N'	$T_1(N')$	$T_2(N')$	$T_3(N')$
0	105 645.016				0	105 641.716		
1	105 648.260	105 648.742	105 638.001		1		105 645.015	
2	105 651.174s			105 633.868	2		105 651.975	105 652.457
3	105 655.520			105 629.675s	3		105 662.319s	
4	105 657.838			105 625.170s	4		105 677.811	
5	105 660.217			105 622.082	5		105 694.988	
6	105 662.45			105 616.99	6		105 715.940	
7				105 611.92	7		105 740.46	

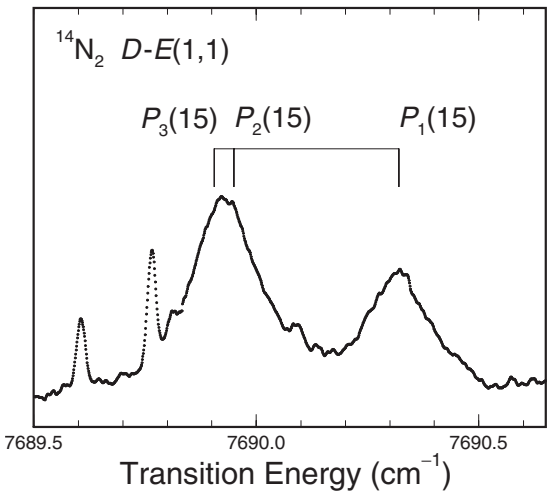

FIG. 5. NIR spectrum in the region of the broadened $P(15)$ lines from the $D-E(1,1)$ band of $^{14}N_2$. Fitted positions for the P_1, P_2, and P_3 lines are indicated. Simultaneously fitted predissociation linewidths are ~0.17 cm^{-1} FWHM for each component. The overlapping narrow lines are from unidentified transitions.

ing the mixing coefficients for $J=4e$ implied by the foregoing local deperturbation analysis, an inherent $o(v=0,J=4e)$ predissociation width of 0.016 cm^{-1} FWHM, and assuming no interference effects in the $D(v=1)\sim o(v=0)$ interaction, it can be inferred that the inherent (deperturbed) predissociation width for $D(v=1,J=4)$ is 0.004 ± 0.002 cm^{-1} FWHM. Thus, there is also the suggestion of significant J dependence in the predissociation of $D(v=1)$ in $^{15}N_2$. Unfortunately, however, the restricted range of rotational levels accessible with the present Doppler-reduced PDA system, together with the uncertainties inherent in the determination of Lorentzian components for near instrument-limited linewidths, do not allow any conclusions to be drawn regarding the functional form of that J dependence.

B. NIR experiment

The NIR spectrum analyzed here covers the range 7586.6–7704.5 cm^{-1}, which contains the strong $c\ ^1\Pi_u - a''\ ^1\Sigma_g^+(1,0)$ band reported elsewhere.[15] It lies between the two spectra at higher and lower energies, analyzed by Kanamori *et al.*, which contained the $D\ ^3\Sigma_u^+ - E\ ^3\Sigma_g^+(0,0)$ and (1,1) bands[6] and the $G\ ^3\Pi_u - E\ ^3\Sigma_g^+(0,0)$ band,[30] respectively. Underlying the $c-a''(1,0)$ band, we have located high-N'' lines from the P branch of the $D-E(1,1)$ band together with the (2,2) and (3,3) bands, all of which are distinguished by their high degree of rotational predissociation.

1. $D(v=1)$ in $^{14}N_2$

In Fig. 5, the NIR spectrum is shown for the $P(15)$ triplet from the $D-E(1,1)$ band. By fitting a sum of three Voigt profiles, with all line centers as free parameters, but with the relative strengths of the P_3 and P_2 lines fixed at the case-(b) value of 0.934,[31] and with a common predissociation width assumed for this line pair, it can be deduced that the P_2-P_3 separation is 0.05(1) cm^{-1} and that the predissociation widths are $\Gamma_1=0.168(4)$ cm^{-1} FWHM and $\Gamma_{23}=0.167(8)$ cm^{-1} FWHM. Transition energies for the $P(12-20)$ lines and corresponding $D(v=1)$ predissociation level widths, determined similarly, are summarized in Table IV. The $D(v=1)$ level widths determined here connect smoothly with the lower-N F_1 results of Kanamori *et al.*,[6,32] and show a continued trend of strong rotational predissociation, with the width increasing by more than two orders of magnitude between $N=1$ and $N=19$. Furthermore, it is evident from Table IV that there is little, if any, dependence of the predissociation widths for a given N on the fine-structure component, at least for the relatively high-N levels studied. This Hund's case-(b) type of behavior is consistent with rotational predissociation by a $^3\Pi_u$ state,[23] the same mechanism suggested by Kanamori *et al.*[6] and pursued in the present CSE study.

Since the high-N'' R-branch lines did not occur in the scanned spectral range, we could not determine independent spectroscopic parameters for $E(v=1)$. Therefore, in order to determine $D(v=1)$ terms, we adopted the $E(v=1)$ B value from Ref. 6, together with the $E(v=0)$ D value and fine-structure splitting parameters of Ref. 30. These latter parameters agree, within the experimental uncertainties, with the $E(v=1)$ parameters of Ref. 6, but are characterized over a greater range of N values, more appropriate when considering the extended results of this work. Spectroscopic param-

TABLE IV. Observed transition energies, in cm^{-1}, and upper-state predissociation level widths, in cm^{-1} FWHM, for the $D\ ^3\Sigma_u^+ - E\ ^3\Sigma_g^+(1,1)$ band of $^{14}N_2$, from NIR spectrum. Separate energies could not be determined for the P_2 and P_3 lines marked with an asterisk. Fitted level widths Γ_{23} assume a common value for the F_2 and F_3 components, while the $\bar{\Gamma}$ assume a common width for all components.

N''	$P_1(N'')$	$P_2(N'')$	$P_3(N'')$	N'	$\Gamma_1(N')$	$\Gamma_{23}(N')$	$\bar{\Gamma}(N')$
12	7703.67	7703.29	7703.25	11	0.090(1)	0.098(3)	
13	7699.28	7698.90	7698.85	12	0.106(2)	0.103(3)	
14	7694.83	7694.45	7694.39	13	0.120(3)	0.129(3)	
15	7690.32	7689.95	7689.91	14	0.168(4)	0.167(8)	
16	7685.76	7685.41	7685.36	15	0.207(6)	0.225(11)	
17	7681.12[a]	7680.82	7680.73	16			0.26(2)
18	7676.49	7676.14*	7676.14*	17			0.31(1)
19	7671.83	7671.41*	7671.41*	18			
20	7667.03	7666.75*[b]	7666.75*[b]	19			0.35(2)

[a]Fitted energy for unresolved broad line underlying strong absorption features; not included in Hamiltonian fit.
[b]Level possibly perturbed; not included in Hamiltonian fit.

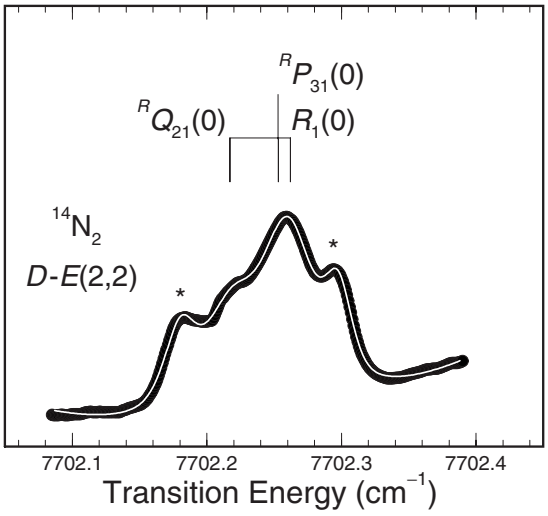

FIG. 6. NIR spectrum in the region of the $R(0)$ line from the $D\ ^3\Sigma_u^+ - E\ ^3\Sigma_g^+(2,2)$ band of $^{14}N_2$ (filled circles), compared with Voigt-profile fit (white curve). Fitted positions for the R-form lines arising from $N''=0$ are indicated, assuming an $R_1(0):{}^RQ_{21}(0):{}^RP_{31}(0)$ strength ratio of 5:3:1, and a common predissociation width. The overlapping, significantly narrower features marked with asterisks are from unidentified transitions.

eters for $D(v=1)$, determined by fitting the $^3\Sigma$ Hamiltonian to the combined terms of Ref. 6 and the present study, are listed in the fourth column of Table II. We note that these parameters differ somewhat from those of Kanamori *et al.*,[6] but not seriously. This N dependence of the parameter set, together with the necessity to include the centrifugal distortion terms λ_D and γ_D in the fit, suggest that $D(v=1)$ may be perturbed. The higher-lying valence levels $b'\ ^1\Sigma_u^+(v=3)$ and the broad $C\ ^3\Pi_u(v=13)$ (Ref. 18) are expected to cross $D(v=1)$ at around $N=15e$ and $N=20ef$, respectively. Indeed, there is evidence from our spectrum that at least one of the $P_3(20)$ and $P_2(20)$ lines is displaced from its expected position.

2. $D(v=2)$ in $^{14}N_2$

Among the strongest lines from the $c-a''(1,0)$ band in the NIR spectrum lie several broadened lines from the $D-E(2,2)$ band. In most cases, the predissociation broadening is such that the lines appear as single peaks. Furthermore, due to overlapping by stronger features, some peaks are not resolvable. Nevertheless, it is possible to characterize the $D(v=2)$ level based on these fragmentary observations.

In Fig. 6, a portion of the NIR spectrum is shown in the region of the $R(0)$ peak of $D-E(2,2)$, which consists of three R-form lines arising from the $N''=0$, $J''=1$ level of $E(v=2)$, i.e., $R_1(0)$, $^RQ_{21}(0)$, and $^RP_{31}(0)$, with strengths in the ratio 5:3:1.[31] By fitting the sum of Voigt profiles to this spectrum, assuming a common Lorentzian width for each of these lines, a predissociation linewidth of 0.044(3) cm^{-1} FWHM can be deduced, together with an $R_1(0)-{}^RQ_{21}(0)$ separation of 0.045(2) cm^{-1}.[33] By far the narrowest peak from the $D-E(2,2)$ band is $P(1)$, which consists of separate transitions from the three $N''=1$ fine-structure levels of $E(v=2)$, i.e., nearly coincident $P_1(1)$ and $^PQ_{21}(1)$ lines with a much weaker $^PR_{13}(1)$ line as a shoulder on the high-energy wing at +0.026(2) cm^{-1} from $P_1(1)$. This latter separation is similar to those observed for the same lines in the $D-E(0,0)$ and (1,1) bands by Kanamori *et al.*,[6] suggesting that the fine structure splitting in the $E(v=0-2)$ levels does not change significantly with v.

Transition energies and upper-state predissociation level widths for the $D-E(2,2)$ band, obtained by fitting Voigt-profile sums to the NIR spectrum, are summarized in Table V. For $N''>1$, all observed peaks are single. For these cases, the least-squares fits were performed to a sum of three Voigt profiles with the fine-structure strength ratios fixed at the case-(b) values,[31] and assuming a common Lorentzian width for each component.[34] The most important result from this analysis, as in the case of $D(v=1)$ discussed in Sec. IV B 1, is the observation of very strong rotational predissociation, evidenced by the level widths in the last column of Table V. In the case of $D(v=2)$, however, the effect is ~35 times stronger. Analysis of the $R(0)-P(2)$ combination difference suggests a value $B=1.888(1)$ cm^{-1} for the $E(v=2)$ rotational constant. Using this value and the other constants employed in Sec. IV B 1 for $E(v=1)$, we determined term values for $D(v=2)$ and fitted them to the $^3\Sigma$ Hamiltonian, yielding the $D(v=2)$ spectroscopic parameters in the penultimate column of Table II.

3. $D(v=3)$ in $^{14}N_2$

Fortuitously, the complete low-N'' structure of the $D-E(3,3)$ band, shown in Fig. 7, is visible in the NIR spec-

TABLE V. Observed transition energies, in cm^{-1}, and upper-state predissociation level widths, in cm^{-1} FWHM, for the $D\ ^3\Sigma_u^+ - E\ ^3\Sigma_g^+(2,2)$ band of $^{14}N_2$, from NIR spectrum. Separate energies could not be determined for the P_2 and P_3 lines marked with an asterisk. Fitted level widths $\bar{\Gamma}$ assume a common width for all fine-structure components.

N''	$P_1(N'')$	$P_2(N'')$	$P_3(N'')$	$R_1(N'')$	N'	$\bar{\Gamma}(N')$
0				7702.261[a]		
1	7694.784[b]				0	~0.001 [c]
2	7690.928	7690.885	7690.971		1	0.042(2)
4	7682.949	7682.895*	7682.895*		3	0.209(12)
6	7674.673	7674.480*	7674.480*		5	0.56(3)
8	7665.958	7665.731*	7665.731*		7	1.08(15)

[a] ${}^RP_{31}(N''=0)=7702.253$; ${}^RQ_{21}(N''=0)=7702.215$.
[b] ${}^PQ_{12}(N''=1)=7694.792$; ${}^PR_{13}(N''=1)=7694.818$.
[c] Approximate width; pertains to F_1 level only.

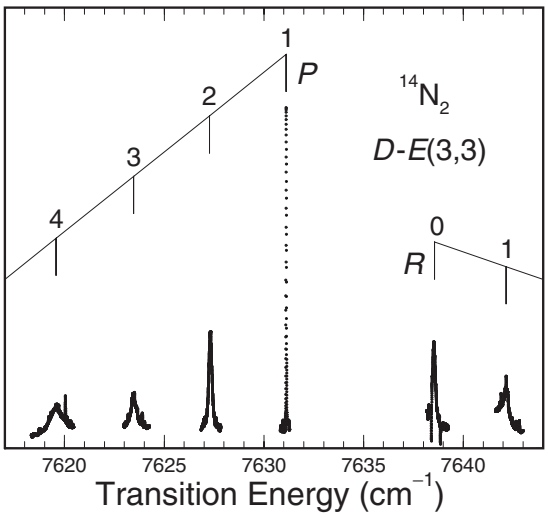

FIG. 7. NIR spectrum of the $D\,^3\Sigma_u^+ - E\,^3\Sigma_g^+(3,3)$ band of $^{14}N_2$, indicating very strong rotational broadening. The overlapping very narrow features are from unidentified neutral and ionic transitions.

trum, displaying the 2:1 even/odd intensity alternation consistent with the nuclear-spin statistics for $^{14}N_2$ and with rapidly increasing rotational broadening clearly evident. Due to this broadening, all peaks are single. Only in the case of the very narrow $P(1)$ peak, which accesses only the F_1 level of $D(v=3,\ N=0)$, is fine-structure information directly available. In this case, the $^PR_{13}$ line appears as a weak shoulder $+0.026(1)$ cm^{-1} from the coincident $P_1(1)$ and $^PQ_{12}(1)$, similar behavior to that found for the same levels in $D(v=2)$ in Sec. IV B 2, suggesting that the v-independence of the $E(v)$ fine-structure splitting extends at least to $v=3$.

Transition energies and upper-state predissociation level widths for the $D-E(3,3)$ band obtained as in Sec. IV B 2 are summarized in Table VI. As in the cases of D ($v=2$ and 3), the level widths summarized in the last column of Table VI indicate very strong rotational predissociation with dependence on N rather than J, i.e., consistent with case-(b) behavior.[23] In the case of $D(v=3)$, however, the effect is strongest, approximately four times stronger than in $D(v=2)$. Analysis of the $R(0)-P(2)$ combination difference suggests a value $B=1.870(2)$ cm^{-1} for the $E(v=3)$ rotational constant. Using this value and the other constants employed in Sec. IV B 1 for $E(v=1)$, we determined term values for $D(v=3)$ and fitted them to the $^3\Sigma$ Hamiltonian, yielding the $D(v=3)$ spectroscopic parameters in the last column of Table II.

C. Vibrational structure

Since the spectroscopic parameters in Table II have been obtained not only from $D-X(v',0)$ spectra, but also from $D-E(v',v''=1,2,3)$ spectra, in order to obtain a coherent picture of the D-state vibrational structure, it is also necessary to address the vibrational structure of the E state.

By using the present $D-X(0,0)$ origin from Table II and the $D-E(0,0)$ origin of Kanamori *et al.*,[6] the electronic energy for $E(v=0)$ is determined to be 95 774.491(7) cm^{-1}, in excellent agreement with the previous value of Carroll and Doheny,[35] 95 774.50(5) cm^{-1}, but significantly more precise.[36] Using standard isotopic polynomial expressions[29] together with the $^{14}N_2$ $D-X(0,0)$ and $^{15}N_2$ $D-X(1,0)$ origins from Table II, one can deduce a precise value of 105 709.5(1) cm^{-1} for the energy of $D(v=1)$ in $^{14}N_2$, with only a very small uncertainty caused principally by the uncertainty in the assumed value of $\omega_e x_e$, taken to be 20(2) cm^{-1} (see below). Together with the $D-E(1,0)$ origin in Table II, this leads to an energy of 97 957.3(1) cm^{-1} for $E(v=1)$ and a vibrational difference $\Delta T_{1/2}=2182.8(1)$ cm^{-1}, some 2 cm^{-1} lower than that implied by the band-head measurements of Carroll and Doheny.[35] These energies and vibrational differences for the D- and E-state levels are summarized in Table VII, together with values extrapolated to $v=2$ and 3, assuming E-state vibrational spacings similar to those of the ionic ground state (final column of Table VII), and using the $D-E$ origins of Table II.

The validity of this extrapolation for the E state depends on the assumption of ionlike behavior, requiring that no large-scale perturbations occur. The experimental rotational constants for the E-state levels (Ref. 6 and Secs. IV B 2 and IV B 3) are well behaved, implying $B_e=1.934$ cm^{-1} and $\alpha_e=0.018$ cm^{-1}, fairly similar to the ionic values and thus supporting this assumption. The fitting of quadratics to the energies of Table VII yields the spectroscopic parameters $T_e=102\,489$ cm^{-1}, $\omega_e=2178$ cm^{-1}, and $\omega_e x_e=21$ cm^{-1} for the D state, and $T_e=94\,671$ cm^{-1}, $\omega_e=2216$ cm^{-1}, and $\omega_e x_e=17$ cm^{-1} for the E state. Therefore, while both states are members of Rydberg series converging on the ground state

TABLE VI. Observed transition energies, in cm^{-1}, and upper-state predissociation level widths, in cm^{-1} FWHM, for the $D\,^3\Sigma_u^+ - E\,^3\Sigma_g^+(3,3)$ band of $^{14}N_2$, from NIR spectrum. Separate energies could not be determined for the lines marked with an asterisk. Fitted level widths $\bar{\Gamma}$ assume a common width for all fine-structure components.

N''	$P_1(N'')$	$P_2(N'')$	$P_3(N'')$	$R_1(N'')$	$R_2(N'')$	$R_3(N'')$	N'	$\bar{\Gamma}(N')$
0				7638.55*[a]				
1	7631.116*[b]			7642.14*	7642.14*	7642.14*	0	0.0065(7)[c]
2	7627.32	7627.27	7627.40				1	0.140(7)
3	7623.46*	7623.46*	7623.52				2	0.35(4)
4	7619.58*	7619.58*	7619.58*				3	0.80(8)

[a] $^RP_{31}(N''=0)=7638.55^*$; $^RQ_{21}(N''=0)=7638.50$.
[b] $^PQ_{12}(N''=1)=7631.116^*$; $^PR_{13}(N''=1)=7631.142$.
[c] Width pertains to F_1 level only.

TABLE VII. Energies for vibrational levels of the $3p\sigma_u D\ ^3\Sigma_u^+$ and $3s\sigma_g E\ ^3\Sigma_g^+$ Rydberg states of $^{14}N_2$, in cm^{-1}. Corresponding vibrational differences are compared with those for the ground state of N_2^+.

v	$T_v(D)$ [a]	$\Delta T_{v+1/2}(D)$	$T_v(E)$ [a]	$\Delta T_{v+1/2}(E)$	$\Delta T_{v+1/2}[X(N_2^+)]$ [b]
0	103 572.667(7)	2136.9(1)	95 774.491(7)	2182.8(1)	2174.7
1	105 709.5(1)	2096(2)[c]	97 957.3(1)	2150(2)[d]	2142.1
2	107 805(2) [c]	2054(5)[c]	100 107(2) [d]	2117(4)[d]	2109.3
3	109 859(4) [c]		102 224(4) [d]		

[a] $T=\nu_0+2\lambda/3-\gamma$, referenced to $X\ ^1\Sigma_g^+(v=0,\ J=0)$.
[b] From the constants in Ref. 3.
[c] From present NIR results and extrapolated E-state energies.
[d] Extrapolated value.

of N_2^+, their level structures differ somewhat, with the D-state levels being significantly compressed compared with those of the more ionlike E state. Indeed, it is the significant difference in $\omega_e x_e$ values for these states which allows the observation of well-separated $D-E(v,v)$ bands in the present NIR spectrum. The level compression of the D state may be partially explained by a strong electrostatic interaction with the higher-lying, repulsive $3\ ^3\Sigma_u^+$ valence state, as discussed in Sec. III.

D. CSE model

1. Model parameters

The initial D-state potential-energy curve was taken to be an energy-shifted version of the diabatic $c\ ^1\Pi_u$ Rydberg curve determined in Ref. 2, which was then shifted and scaled linearly in two dimensions in order to minimize the residuals in the least-squares model fit to the experimental database. The resultant fitted diabatic-basis potential-energy curve for the D state shown in Fig. 8 is consistent with expectation for the lowest member of a Rydberg series converging on the ionic ground state, yielding the following diabatic spectroscopic parameters: $\omega_e=2179\ cm^{-1}$, $\omega_e x_e=21\ cm^{-1}$, $T_e=102\ 488\ cm^{-1}$, i.e., similar to the adiabatic parameters given in the previous section, together with $B_e=1.933\ cm^{-1}$, $\alpha_e=0.026\ cm^{-1}$, and $\gamma_e=0.003\ cm^{-1}$. Due to the incomplete experimental characterization of the $D(v=2,3)$ levels, the potential is increasingly uncertain in detail above $\sim 107\ 000\ cm^{-1}$. For completeness, the model diabatic potential-energy curves for the $^3\Pi_u$ states are shown in Fig. 9, emphasizing the complexity of the predissociating manifold.

The fitted diabatic heterogeneous coupling $\eta=1.40(2)\ cm^{-1}$ is determined quite precisely through its control of the rotational predissociation of the D-state levels, which is well characterized experimentally. This value is in excellent agreement with the single-electron value $\langle 3p\pi_u|\mathbf{l}^+|3p\sigma_u\rangle=\sqrt{2}$ expected for the case of diabatic-basis pure precession applicable to the interaction between the $\sigma_g 3p\sigma_u D\ ^3\Sigma_u^+$ and $\sigma_g 3p\pi_u G\ ^3\Pi_u$ states of this $3p$ Rydberg complex.[21] The fitted diabatic spin-orbit coupling $\xi=1.0(3)\ cm^{-1}$ is determined only approximately, manifesting experimentally mainly in the F_1 level width for $D(v=3,\ N=0)$, which is significantly narrower than the instrumental resolution of the NIR spectrum and thus is subject to some uncertainty. In the case of the $\sigma_g 3p\sigma_u D\ ^3\Sigma_u^+$ and $\sigma_g 3p\pi_u G\ ^3\Pi_u$ states, the spin-orbit interaction $\xi\approx A_G$, the diabatic spin-orbit constant of the G state, expected to be on the order of $+2\ cm^{-1}$,[11] which is rough agreement with the observed value of ξ. This small value is expected for Rydberg states built on a core of Σ symmetry due to the spin-orbit constant being defined solely by the diffuse $3p\pi_u$ mo-

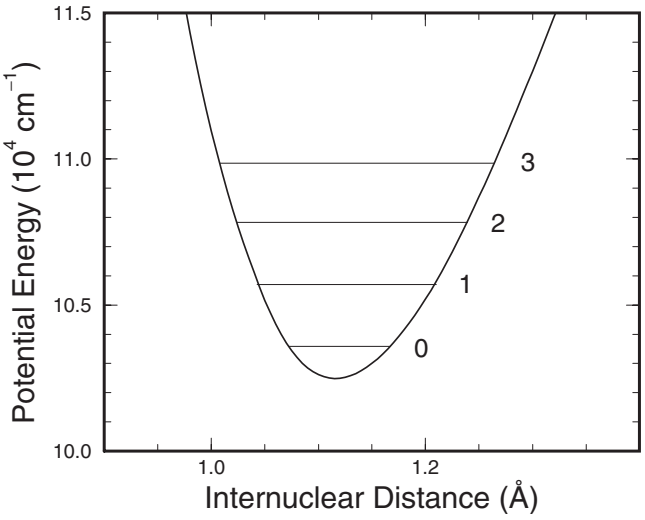

FIG. 8. Model diabatic potential-energy curve for the $D\ ^3\Sigma_u^+$ state of N_2, relative to the $v=0$, $J=0$ level of the $X\ ^1\Sigma_g^+$ state. Observed energies for the $D(v=0-3)$ levels of $^{14}N_2$ are also shown.

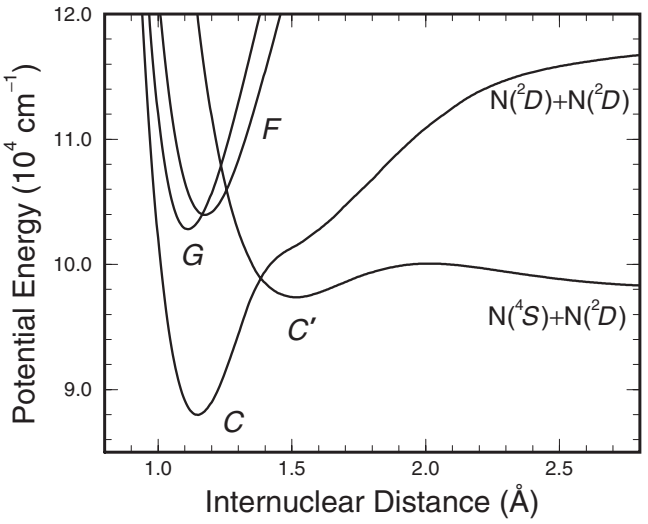

FIG. 9. Model diabatic potential-energy curves for the $^3\Pi_u$ Rydberg-valence manifold of N_2, taken from Ref. 18.

TABLE VIII. Comparison of experimental, diabatic, and coupled-channel spectroscopic parameters for levels of the $D\ ^3\Sigma_u^+$ state of N_2, all in cm^{-1}.

Iso.	v	T_{exp}	T_{dia}	T_{CSE}	ΔT [a]	B_{exp}	B_{dia}	B_{CSE}	ΔB [b]
$^{14}N_2$	0	103 572.7	103 572.43	103 572.46	0.03	1.961	1.921	1.961	0.040
	1	105 709.5	105 709.28	109 709.27	−0.01	1.883	1.899	1.882	−0.017
	2	107 805	107 805.42	107 805.40	−0.02	1.842	1.885	1.846	−0.039
	3	109 859	109 858.42	109 858.40	−0.02	1.843	1.874	1.839	−0.035
$^{15}N_2$	1	105 641.8	105 641.83	105 641.82	−0.01	1.760	1.774	1.760	−0.014

[a] $\Delta T = T_{CSE} - T_{dia}$.
[b] $\Delta B = B_{CSE} - B_{dia}$.

lecular orbital, together with the $1/r^3$ dependence of the spin-orbit operator.[21] While it is not possible here to determine the signs of the off-diagonal matrix elements η and ξ absolutely, their relative signs determine the relative magnitudes of the triplet-fine-structure predissociation widths, with the ordering $\Gamma_1 < \Gamma_2 < \Gamma_3$ expected for $\eta\xi > 0$.[23] The present fitting procedure suggests that $\eta\xi > 0$ as implied by p-complex theory.[21] This conclusion is also supported by Fig. 7 of Ref. 6, where it can be seen that the F_1 component of the $D(v=1,\ N=2)$ triplet has the narrowest width.

2. Energies and widths

In Table VIII, the spectroscopic database employed in the fitting procedure (columns 3 and 7) is compared with the final CSE-model calculations (columns 5 and 9), showing very satisfactory agreement. The experimental energies are reproduced by the model to within $\pm 0.2\ cm^{-1}$ or the experimental uncertainty, whichever is the greater, while the worst discrepancy for the rotational constants is $\pm 0.004\ cm^{-1}$, equivalent to the 2σ uncertainty level in the case of $D(v=2)$ for $^{14}N_2$. Uncoupled (diabatic) energies and rotational constants are also shown in columns 4 and 8 of Table VIII, allowing the calculation of shifts due to the $D \sim G$ couplings, shown in columns 6 and 10. The shifts in energy are very small, reflecting the minor role of the homogeneous coupling. However, it is worth noting that the $\lambda = -0.5\Delta T$ contributions implied by these shifts can in no way explain the larger observed λ values in Table II. It is likely that singlet states will need to be added to the CSE model in order to completely explain the triplet fine-structure splitting. This is beyond the scope of the present work. The important role of the heterogeneous coupling is indicated by the significant perturbations in B shown in the final column of Table VIII, which display a change in sign between $v=0$ and 1. The upward shift in B for $D(v=0)$ is related to a similar downward shift for $G(v=0)$, but in this latter case the situation is further complicated by heavy mixing between the G and F states.[18]

The main theoretical result of this work is shown in Fig. 10, where CSE-model predissociation widths for the $D(v=1-3)$ levels of $^{14}N_2$ are compared with the present experimental results and those of Ref. 6, over the full ranges of N accessed experimentally. The model widths show a small dependence on the fine-structure component, with $\Gamma_1 < \Gamma_2 < \Gamma_3$, the differences decreasing as N increases, as expected in the Hund's case-(b) limit.[23] The model F_2 widths are in excellent agreement with the fine-structure-averaged experimental widths for $D(v=1,2)$, but exceed the experimental values by ~30% for $D(v=3)$, in which case the F_1 widths are in much better agreement, possibly because these low-N experimental widths might be more representative of the more intense F_1 component. Overall, the enormous increase in predissociation with both vibration and rotation is reproduced outstandingly well by the model, achieved essentially by using only one adjustable parameter, i.e., η. The value of ξ was adjusted to reproduce the experimental F_1 width of $0.0065\ cm^{-1}$ FWHM listed in Table VI for $D(v=3,\ N=0)$, leading to the model value for ξ quoted in Sec. IV D 1. The corresponding model width calculated for the $D(v=2,\ N=0)$ level is $0.0016\ cm^{-1}$ FWHM, in satisfactory agreement with the $\sim 0.001\ cm^{-1}$ FWHM experimental estimate in Table V. Finally, the computed F_2 width for the $D(v=1,\ N=4)$ level of the $^{15}N_2$ isotopomer, $0.0055\ cm^{-1}$ FWHM, is also in satisfactory agreement with the experimental width of $0.004(2)\ cm^{-1}$ FWHM estimated in Sec. IV A 2.

Due to the strong multichannel couplings within the $^3\Pi_u$ manifold, the dominant rotational predissociation does not display a strictly quadratic dependence on the rotational quantum number. We have therefore fitted polynomials of the form $\Gamma(N=J) = \Gamma_0 + \Gamma_J J(J+1) + \Gamma_{JJ}[J(J+1)]^2 + \Gamma_{JJJ}[J(J+1)]^3$

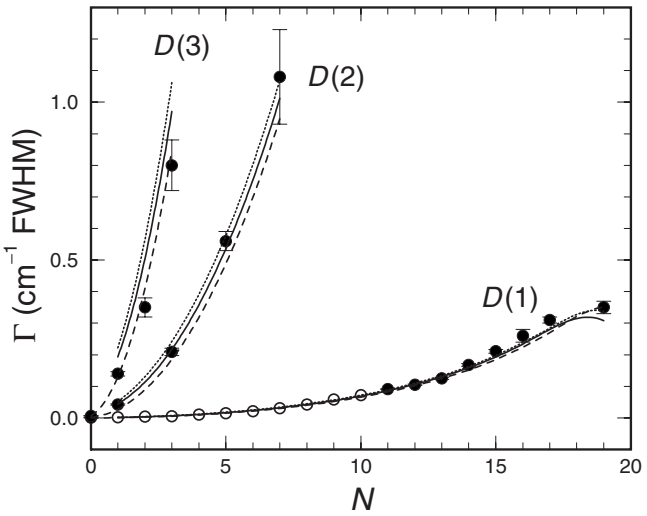

FIG. 10. Vibrational and rotational dependence of predissociation level widths for the $3p\sigma_u D\ ^3\Sigma_u^+$ Rydberg state of $^{14}N_2$. Full circles: Present fine-structure-averaged experimental widths. Open circles: F_1 widths of Ref. 6. Curves: Present CSE-model results (Solid: F_2, dashed: F_1, and dotted: F_3). The turning over of the $D(v=1)$ model widths in the region of $N=19$ is caused by the crossing of $D(v=1)$ in this region by the higher-lying valence level $C\ ^3\Pi_u(v=13)$ which has a lower rotational constant.

TABLE IX. Polynomial coefficients for the generation of CSE-model F_2 predissociation widths for the $D(v=0-3)$ levels of $^{14}N_2$. $\Gamma(N=J)=\Gamma_0+\Gamma_J J(J+1)+\Gamma_{JJ}[J(J+1)]^2+\Gamma_{JJJ}[J(J+1)]^3$ cm^{-1} FWHM; $1\leq J\leq J_{max}$.

v	Γ_0	Γ_J	Γ_{JJ}	Γ_{JJJ}	J_{max}
0	4.2×10^{-6}	1.015×10^{-5}	-9.283×10^{-8}	2.176×10^{-10}	8
1	0.000 37	0.000 516	7.843×10^{-7}	1.708×10^{-9}	17
2	0.0096	0.0171	1.366×10^{-5}		7
3	0.039	0.0769	6.384×10^{-5}		5

to the CSE-model F_2 predissociation widths for the $D(v=0-3)$ levels of $^{14}N_2$, listing the resultant coefficients in Table IX. The Γ_J coefficients listed in the third column of the table emphasize the nearly four orders of magnitude spanned by the rotational predissociation as v increases from 0 to 3.

The rotational dependence of the F_2 widths for $D(v=0)$ computed using the CSE model was found to be anomalous, leading to the restricted range of rotation applicable to the corresponding polynomial coefficients in Table IX. The full CSE-model widths for $D(v=0)$ are shown in Fig. 11, displaying a strong knee near $N=15$, which is associated with a crossing in this region by the broad, higher-lying $C\ ^3\Pi_u(v=10)$ valence level, which has a lower rotational constant. The perturbation associated with this crossing evidently has a strong effect on the $D(v=0)$ predissociation. The model $D(v=0)$ predissociation widths are consistent with the limited experimental information available. First, Γ ranges from 0.000 02 cm^{-1} FWHM at $N=1$ to 0.0004 cm^{-1} FWHM at $N=10$, compatible with the total linewidth of $\sim$0.0004 cm^{-1} FWHM implied by the lifetime measured by Kurzweg *et al.*[28] and suggesting that predissociation becomes competitive with radiative decay near $N=10$. Second, $\Gamma\lesssim0.002$ cm^{-1} FWHM for $N\lesssim14$, consistent with the lack of observation of broadening at this level by Kanamori *et al.*[6] over a comparable range of rotation. Finally, we have found some evidence in the NIR spectrum for the predicted increase in broadening at high N in Fig. 11. Two lines in the spectrum at 7699.88 and 7700.10 cm^{-1}, which are near the expected position for $P_i(32)$ triplet lines from the $D-E(0,0)$ band, have been found to be broadened to an extent incompatible with nearby lines from other bands in this region, with widths of 0.017(4) cm^{-1} FWHM and 0.022(6) cm^{-1} FWHM, respectively. These widths, which plotted as solid circles in Fig. 11 and tentatively associated with the $N=31$ level of $D(v=0)$, are found to be in good agreement with the CSE-model predictions.

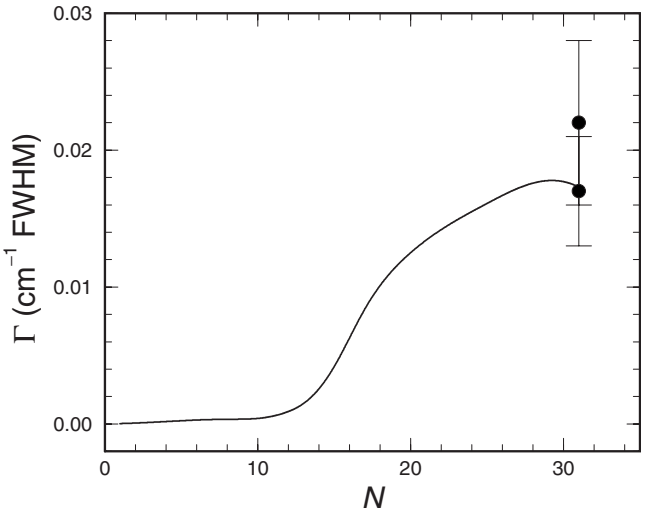

FIG. 11. Rotational dependence of predissociation width for the $D(v=0)$ level of $^{14}N_2$. Solid curve: Computed CSE-model widths for the F_2 sublevel. Solid circles: Experimental linewidths from NIR spectrum for $P_i(32)$ lines from $D-E(0,0)$ band (see text).

The least satisfactory aspect of the CSE-model results is the slight overestimate of the $D(v=3)$ predissociation widths. Contributing factors to this discrepancy are likely to include uncertainties in the large experimental widths due to lack of knowledge of the fine-structure composition and splittings, together with uncertainties in the upper part of the adopted D-state diabatic potential-energy curve due to incomplete knowledge of the $D(v=2,3)$ absolute energy levels. However, in addition, there is a persistent tendency for the effect of the $D\sim G$ couplings on $D(v=3)$ to be too large, resulting in overestimates of both Γ and ΔB, the latter perhaps contributing to some distortion of the D-state model potential, resulting in the unusually large value of γ_e. The probable reason for this problem relates specifically to the $^3\Pi_u$ manifold: It has been pointed out in Ref. 18 that the CSE model of the interacting Rydberg and valence states of $^3\Pi_u$ symmetry is not expected to be valid in the energy region above the $v=3$ Rydberg complex. Further experimental studies and the inclusion of more $^3\Pi_u$ basis states in the CSE model may help to clarify this matter. Indeed, the present model indicates that the $D(v=4)$ level should be far less predissociated than $D(v=3)$, leading to some hope that the $D-E(4,4)$ band may be detectable in new NIR spectra.

V. SUMMARY AND CONCLUSIONS

The $3p\sigma_u D\ ^3\Sigma_u^+$ Rydberg state of N_2 has been studied experimentally using two high-resolution spectroscopic techniques. First, the forbidden $D\ ^3\Sigma_u^+-X\ ^1\Sigma_g^+$ transition has been observed for the first time, via the (0,0) band of $^{14}N_2$ and the (1,0) band of $^{15}N_2$, using 1 XUV +1 UV two-photon-ionization laser spectroscopy. Second, the Rydberg–Rydberg transition $D\ ^3\Sigma_u^+-E\ ^3\Sigma_g^+$ has been studied using NIR diode-laser photoabsorption spectroscopy, thus extending the previous measurements of Kanamori *et al.*[6] to higher transition energies and revealing the (2,2) and (3,3) bands. The combined results show that the $D(v=0-3)$ levels exhibit rapidly increasing rotational predissociation as v increases, spanning nearly four orders of magnitude. The D-state level structure and rotational predissociation signature have been explained quantitatively by means of a coupled-channels model which considers the electrostatically coupled $^3\Pi_u$ Rydberg-valence

manifold, together with a pure-precession **L**-uncoupling rotational interaction between the $3p\sigma_u D\ ^3\Sigma_u^+$ and $3p\pi_u G\ ^3\Pi_u$ Rydberg p-complex components.

ACKNOWLEDGMENTS

This investigation was partially supported by the Molecular Atmospheric Physics (MAP) program of the Netherlands Foundation for Fundamental Research on Matter (FOM) and Australian Research Council Discovery Program Grant Nos. DP0558962 and DP0773050. K.G.H.B. was supported by the Scientific Visits to Europe Program of the Australian Academy of Science. The authors thank Professor H. Kanamori for discussions on his results for the $D(v=1)$ level of $^{14}N_2$ and Professor H. Lefebvre-Brion for her critical reading of the manuscript.

[1] M.-C. Liang, A. N. Heays, B. R. Lewis, S. T. Gibson, and Y. L. Yung, Astrophys. J. **664**, L115 (2007).
[2] B. R. Lewis, S. T. Gibson, W. Zhang, H. Lefebvre-Brion, and J.-M. Robbe, J. Chem. Phys. **122**, 144302 (2005).
[3] A. Lofthus and P. H. Krupenie, J. Phys. Chem. Ref. Data **6**, 113 (1977).
[4] G. Joyez, R. I. Hall, J. Reinhardt, and J. Mazeau, J. Electron Spectrosc. Relat. Phenom. **2**, 183 (1973).
[5] A. B. van der Kamp, P. C. Cosby, and W. J. van der Zande, Chem. Phys. **184**, 319 (1994).
[6] H. Kanamori, S. Takashima, and K. Sakurai, J. Chem. Phys. **95**, 80 (1991).
[7] H. Lefebvre-Brion and C. M. Moser, J. Chem. Phys. **43**, 1394 (1965).
[8] P. Cremaschi, A. Chattopadhyay, P. V. Madhavan, and J. L. Whitten, Chem. Phys. **109**, 117 (1986).
[9] H. H. Michels, Adv. Chem. Phys. **45**, 225 (1981).
[10] B. Minaev, P. Norman, D. Jonsson, and H. Ågren, Chem. Phys. **190**, 11 (1995).
[11] J. P. Sprengers, E. Reinhold, W. Ubachs, K. G. H. Baldwin, and B. R. Lewis, J. Chem. Phys. **123**, 144315 (2005).
[12] B. R. Lewis, K. G. H. Baldwin, J. P. Sprengers, W. Ubachs, G. Stark, and K. Yoshino, J. Chem. Phys. **129**, 164305 (2008).
[13] J. P. Sprengers, W. Ubachs, K. G. H. Baldwin, B. R. Lewis, and W.-Ü. L. Tchang-Brillet, J. Chem. Phys. **119**, 3160 (2003).
[14] J. P. Sprengers, W. Ubachs, and K. G. H. Baldwin, J. Chem. Phys. **122**, 144301 (2005).
[15] Y. Kawamoto, M. Fujitake, and N. Ohashi, J. Mol. Spectrosc. **185**, 330 (1997).
[16] E. F. van Dishoeck, M. C. van Hemert, A. C. Allison, and A. Dalgarno, J. Chem. Phys. **81**, 5709 (1984).
[17] Since the D-X transition is spin-forbidden, the nonzero CSE cross section, resulting from the selection of a D-X electronic transition moment of unity, is artificial.
[18] B. R. Lewis, A. N. Heays, S. T. Gibson, H. Lefebvre-Brion, and R. Lefebvre, J. Chem. Phys. **129**, 164306 (2008).
[19] H. Ndome, M. Hochlaf, B. R. Lewis, A. N. Heays, S. T. Gibson, and H. Lefebvre-Brion, J. Chem. Phys. **129**, 164307 (2008).
[20] J. W. C. Johns and D. W. Lepard, J. Mol. Spectrosc. **55**, 374 (1975).
[21] H. Lefebvre-Brion and R. W. Field, *The Spectra and Dynamics of Diatomic Molecules* (Elsevier, Amsterdam, 2004), pp. 97, 144, 181–185, and 330.
[22] I. Kovács, *Rotational Structure in the Spectra of Diatomic Molecules* (Hilger, London, 1969), pp. 258–260.
[23] P. S. Julienne, J. Mol. Spectrosc. **56**, 270 (1975).
[24] B. R. Lewis, P. M. Dooley, J. P. England, K. Waring, S. T. Gibson, K. G. H. Baldwin, and H. Partridge, Phys. Rev. A **54**, 3923 (1996).
[25] In the case of the **L**-uncoupling interaction between the e-parity levels of $^3\Pi_0$ and $^3\Sigma_1^+$, the sign is reversed.
[26] J. Bendtsen, J. Raman Spectrosc. **2**, 133 (1974).
[27] A. S.-C. Cheung, K. Yoshino, W. H. Parkinson, and D. E. Freeman, J. Mol. Spectrosc. **119**, 1 (1986).
[28] L. Kurzweg, G. T. Egbert, and D. J. Burns, J. Chem. Phys. **59**, 2641 (1973).
[29] G. Herzberg, *Molecular Spectra and Molecular Structure I. Spectra of Diatomic Molecules* (Van Nostrand, Princeton, 1950), pp. 142–144.
[30] T. Hashimoto and H. Kanamori, J. Mol. Spectrosc. **235**, 104 (2006).
[31] J. B. Tatum and J. K. G. Watson, Can. J. Phys. **49**, 2693 (1971).
[32] In a private communication, Professor Kanamori has indicated that the widths in Fig. 8 of Ref. 6 should be reduced by a factor of 5 for correct comparison with the FWHM results of this work.
[33] The fitted position for the weakest, unresolved line $^RP_{31}(0)$ is somewhat more tentative.
[34] The assumption of equal fine-structure widths for the analysis is likely to be least valid for the lowest-N levels (see, e.g., Ref. 23).
[35] P. K. Carroll and A. P. Doheny, J. Mol. Spectrosc. **50**, 257 (1974).
[36] The electronic energies employed in this work are given by $T=\nu_0 +2\lambda/3-\gamma$, where the ν_0 are the band origins of the Ref. 27 Hamiltonian.